Sensors & Transducers Journal, Vol. 137, Issue 2, February 2012, pp. 165-175

www.sensorsportal.com

Sensors & Transducers

ISSN 1726-5479

http://www.sensorsportal.com

Preparation and Study of Acetone Gas Sensing Behavior of nanocrystalline $LaCrO_3$ Thick Film

[a*] S. M. KHETRE, [a] C. J. KHILARE, [b] V. S. SHIVANKAR, [c] S. R. BAMANE

[a] Dahiwadi College Dahiwadi, Tal. Man, Dist. Satara, (M.S.) 415508, India

[b] Modern College Vashi, Navi-Mumbai (M.S.) India

[c] Metal Oxide Research Laboratory, Dr. Patangrao Kadam College Sangli, (M.S.) 416416, India

Tel: +91 02165220231, fax: 02165220231

E-mail: sanjaykhetre@gmail.com

Received: 14 January 012 /Accepted: 14 February 2012 /Published: 28 February 2012

Abstract: The preparation, characterization and gas sensing properties of pure nanocrystalline $LaCrO_3$ mixed oxide semiconductors have been investigated. The mixed oxides were obtained by mixing lanthanum nitrate, chromium nitrate and glycine in the 1:1:2 proportions respectively. Synthesized materials were characterized by X-ray diffraction (XRD), Infrared spectroscopy (IR), scanning electron microscopy (SEM) and transmission electron microscopy (TEM). $LaCrO_3$ was observed to be sensitive to acetone gas. Upon exposure to acetone gas, the barrier height of $LaCrO_3$ intergranular regions decreases markedly due to the chemical transformation of $LaCrO_3$ into well conducting electrons leading to a drastic decrease in resistance. The crucial gas response 200 ppm was found to acetone gas at 200 ^{0}C and no cross response was observed to other hazardous and polluting gases. The effects of microstructure on the gas response, selectivity, response and recovery of the sensor in the presence of acetone gas were studied and discussed.

Keywords: Nanocrystalline $LaCrO_3$, XRD, Thick film resistor, Acetone, Gas sensor.

1. Introduction

Metal oxide semiconductor gas sensors have found increasing application in domestic, commercial and industrial gas sensing systems through environmental pollution monitoring, detection of harmful gases in mines, grading of food and agro-products, home safety to hand held breath analyzers etc. [1-3]. It plays a positive role in inspecting and monitoring harmful and inflammable gases. Due to the advantages of small size, simple operation, low cost and good reversibility, the semiconductor sensors

have become the most promising devices among the solid-state chemical sensors. Many semiconductor oxides such as ZnO, SnO_2, Fe_2O_3, In_2O_3, WO_3, and CuO, have been explored to detect the polluting, toxic and inflammable gases [4-6]. Furthermore, several metal oxides with the perovskite structure and of the form ABO_3 (A= lanthanide or alkaline earth metal, B = transition metal) were used as gas-sensing materials to detect toxic and combustible gases, such as CO, H_2S, LPG, acetone and alcohol [7-12]. Thick film sensors that do not require a reference cell are simpler and thus less expensive to manufacture. Moreover, the time response can be reduced, providing for increased speed [13]. In this regard, mixed metal oxide $LaCrO_3$ thick film is an interesting material system. Recently, a lot of interest was focused on the synthesis/processing and characterization of nanoscale mixed oxide ceramic. A fine particle with dimensions of less than 100 nm ceramic materials have potential applications in many technology areas due to their crucial microstructure-based properties and especially in the fabrication of nanoscale devices is of intense scientific and technological interest[14]. The aim of this work was to study the acetone gas-sensing properties of $LaCrO_3$ synthesized by combustion method.

2. Experimental

Analytical grade $La(NO_3)_3 \cdot 6H_2O$, $Cr(NO_3)_3 \cdot 9H_2O$ and $C_2H_5NO_2$ were used as raw materials to prepare $LaCrO_3$. According to the stoichiometric preparation of the reactants, the specified amounts of Fe $(NO_3)_3 \cdot 9H_2O$ and Cr $(NO_3)_3 \cdot 6H_2O$ were first dissolved in glycine solution to form the sol. The molar amount of glycine was double to total molar amount of metal nitrates in the solution. A small amount of ammonia aqueous was slowly added to adjust the pH to 7. During this procedure, the solution was continuously stirred and kept at a temperature of 60-70 ^{0}C. Then, the stabilized nitrate–glycine sol was poured into a tray and heated slowly to 140-150 ^{0}C.Viscosity and color changed as the sol turned into a green, puffy, porous dry gel. When ignited at any point of the dried gel in air at room temperature, the dried gel simultaneously burnt in a self-propagating combustion manner until they were completely transformed into loose powders, known as as-synthesis powder. The entire combustion process would last a few seconds. The as-synthesis powder was the nanocrystalline $LaCrO_3$ with fine crystal structure.

2.1. Thick Film Preparation

The thixotropic paste was screen printed on a glass substrate in desired patterns [14]. The films prepared were fired at 550 ^{0}C for 24 h. These films were surface modified by dipping them into a 0.01 M aqueous solution of cupric chloride for different intervals of time and were dried at 80 ^{0}C followed by firing at 550 ^{0}C for 24 h in air ambient. The $CuCl_2$ dispersed on the films was oxidized in firing process, and sensor elements with different mass% of $LaCrO_3$ were obtained. Silver contacts were made by vacuum evaporation for electrical measurements. [15].

2.2. Characterization

X-ray diffraction (CrK_α, Philips analytical XRD B.V.PW-1710) was used for confirming the phase and structural study. Infrared spectra (IR) for the synthesis powder were performed on a Perkin-Elmer 883 spectrophotometer from 450 to 4000 cm^{-1}. The surface morphological features were observed by using scanning electron microscopy (JSM-6360A). Transmission electron microscopy (TEM) of the powder was carried out by Make Philips CM-200 superwinster spectrometer at 200 kV. The specific surface area of the powders was measured by BET isotherm technique with nitrogen absorption. Thickness measurements were carried out using a Taylor- Hobson (Talystep, UK) system. Electrical and gas sensing characteristics were measured using a static gas sensing system. The I-V character and

thermoelectric measurement of nanocrystalline $LaCrO_3$ were carried out. The dc resistivity was measured by the two probe method as a function of temperature (room temperature to 550 °C.)

2.3. Details of the Gas Sensing System

The sensing performance of the sensors was examined using a static gas sensing system. There were electrical feeds through the base plate. The heater was fixed on the base plate to heat the sample under test up to required operating temperatures. The current passing through the heating element was monitored using a relay with adjustable ON and OFF time intervals. A Cr–Al thermocouple was used to sense the operating temperature of the sensor. The output of the thermocouple was connected to a digital temperature indicator. A gas inlet valve was fitted at one of the ports of the base plate. The required gas concentration inside the static system was achieved by injecting a known volume of test gas using a gas-injecting syringe. A constant voltage was applied to the sensor, and current was measured by a digital picoammeter. Air was allowed to pass into the glass dome after every acetone gas exposure cycle.

3. Results and Discussion

3.1. XRD Analysis

Formation of the desired $LaCrO_3$ perovskite was confirmed by X-ray diffraction analysis. The XRD pattern shown in Fig. 1 depicts broad peaks due to the nanosized of particles and matches with the reported JCPDS (Card No.24-1016) data. It is well known that, lanthanum chromate (1 1 2) reflection is more intense in the orthorhombic perovskite structures. No unidentified peaks are observed. The orthorhombic perovskite structure of $LaCrO_3$ have the lattice parameters $a = 5.586$ Å and $b = 5.488$ Å, $c = 7.758$ Å ($c/a = 1.388$) respectively. The lattice parameters of the materials are almost equal to those of the constituent phases, indicating that no structural changes have been observed during sintering process. The average crystalline size (t) was calculated using Scherrer's equation $t = 0.9\ \lambda / \beta \cos\theta$ [16-19] where, t is the average crystalline size of the particles, assuming particles to be spherical $K = 0.9$, λ the wavelength of X-ray radiation, β the full width at half maximum of the diffracted peak and θ is the angle of diffraction. The average crystalline size obtained for $LaCrO_3$ calcinated at 850^0C was found to be ~24 nm.

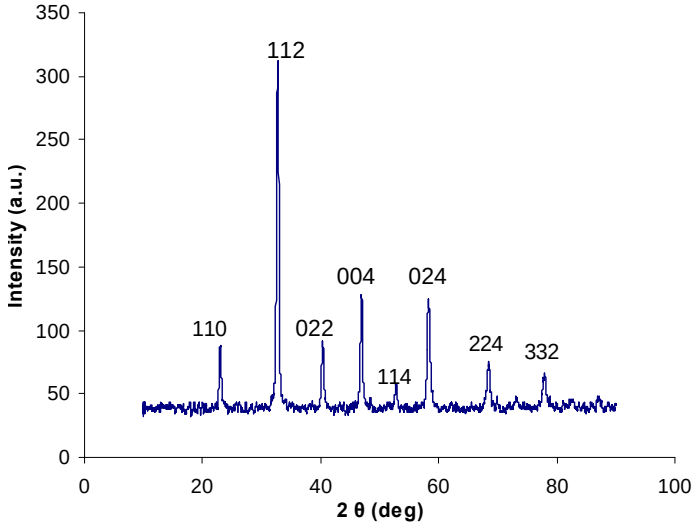

Fig. 1. X-ray diffraction patterns of $LaCrO_3$ as synthesized powder.

3.2. IR Analysis

Fig. 2 shows the FT-IR spectrum of the product, there is one strong absorptive band at about 571 cm^{-1} which correspond to Cr–O stretching vibration and O–Cr–O bending vibration of perovskite $LaCrO_3$ [20-21]. We can see there are characteristic bands at 3422 cm^{-1} of the hydroxyl group due to bound water molecules and the peak at 2922 cm^{-1} is due to ambient CO_2 .This finding proves the formation of the perovskite $LaCrO_3$ and is in accordance with the XRD data. Also, in the FT-IR spectrum of $LaCrO_3$ nanopowder weak bands were observed in the 1465 cm^{-1} region which are attributable to carbonate groups [22]. But, these carbonates were not detected by XRD. Therefore, it is concluded that the carbonates the perovskite-type $LaCrO_3$ by IR are formed mainly on the surface due to exposure to ambient air. The surface of the $LaCrO_3$ particles obtained from the decomposition of the heteronuclear compound is more active to chemisorption of gases such as CO_2 in ambient, leading to the formation of carbonate ions [23]. It is well-known that the catalytic activity and the gas sensing characteristics of $LaCrO_3$ are strongly influenced by particle size [24-25]. Therefore, it is of paramount importance to characterize the microstructure of the powders obtained.

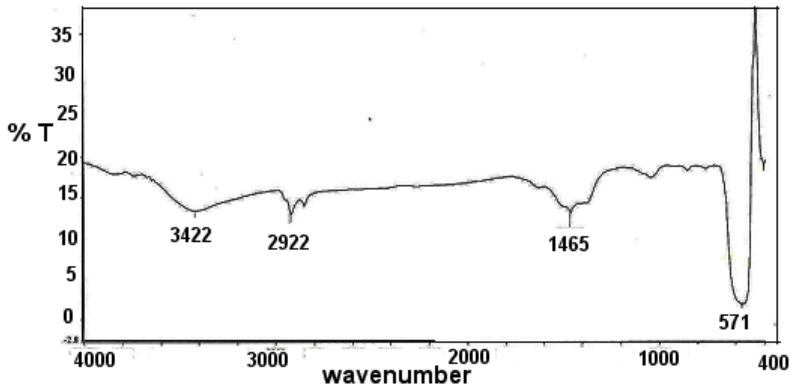

Fig. 2. FTIR spectrum of $LaCrO_3$ powder.

3.3. Microstructure-SEM

The SEM technique was employed for finding morphology of $LaCrO_3$ as synthesized powder Fig. 3. One can notice the presence of macro-agglomerations of very fine particles having size less than 1 μm. The particle shapes are not well defined. Many large and small pores are present in the whole material. We assumed that the pores are mainly intergranular because intragranular pores are not seen on the SEM photograph.

3.4. Microstructure-TEM

The TEM specimen was prepared by placing microdrops of colloids solution on a carbon film supported by a copper grid. To get better understanding and clarity of the morphology the TEM image was taken which validate nearly uniform spherical particles, polymeric linkage with average size of 19-24nm.The agglomeration, as seen in the SEM image was not observed here; on the contrary the image shows distinct nanoparticles of nearly spherical structure and clear boundaries Fig 4 (b-c). The HRTEM image Fig. 4 (d) shows well developed lattice fringes, which are correlated well with the XRD results. The selected area diffraction (SAED) pattern Fig. 4 (a) shows the spot type pattern which is indicative of single crystalline particles. No evidence was found for more than one pattern, suggesting the single phase nature of the material. Surface are of the powder was found to be 3.5 m^2/g.

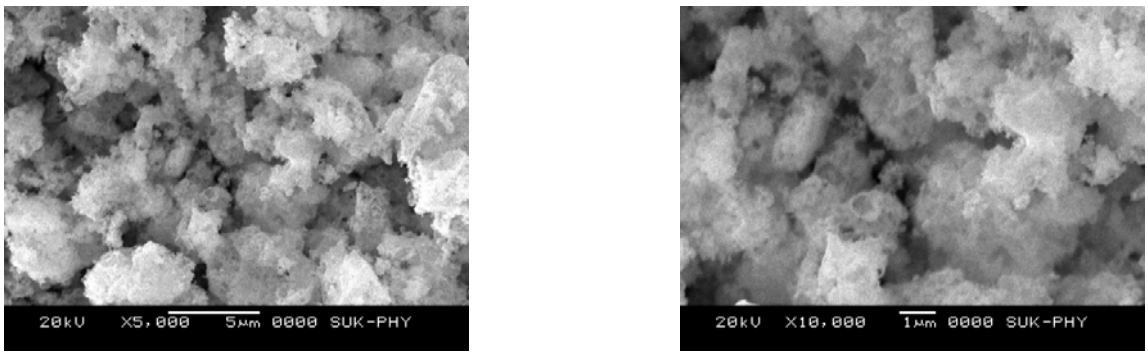

(a) (b)

Fig. 3. SEM micrographs for nanocrystalline $LaCrO_3$.

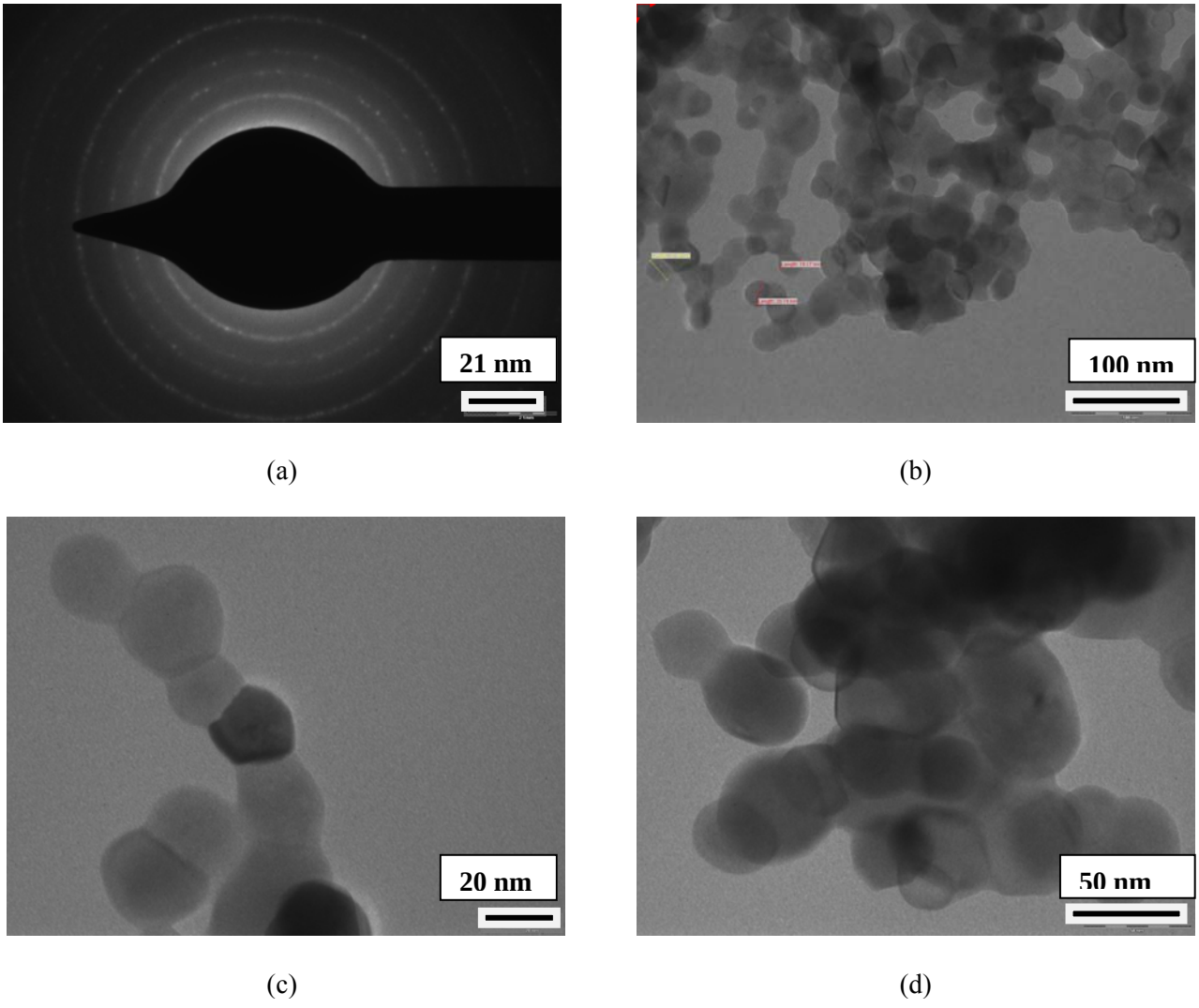

(a) (b)

(c) (d)

Fig. 4. Transmission electron microscopy image of $LaCrO_3$, (a) selected area electron diffraction pattern, (b-c) high resolution transmission electron microscopy image of nanocrystalline $LaCrO_3$, (d) The HRTEM image.

3.5. Thickness Measurement

The thicknesses of the films were observed to be in the range from 30 to 40 µm. The reproducibility of the film thickness was achieved by maintaining the proper rheology and thixotropy of the paste.

3.6. Thermoelectric Power Measurements

The p-type semiconductivity of thick films of $LaCrO_3$ was confirmed by measuring thermoelectromotive force of the thick film samples. The $LaCrO_3$ was observed to be p-type material.

4. Electrical Properties

4.1. I-V Characteristics

Fig. 5 depicts the I–V characteristics of the $LaCrO_3$ films at room temperature. It was clear from the I–V characteristics that the sliver contacts fabricated on the film were ohmic in nature. The voltage applied was in the range 1–30 V.

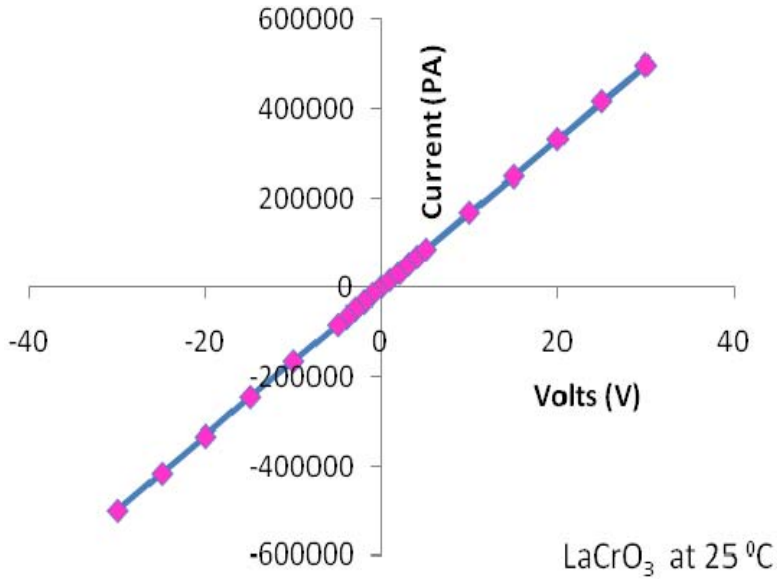

Fig. 5. I-V characteristics of $LacrO_3$.

4.2. Electrical Conductivity

The semiconducting nature of $LaCrO_3$ is observed from the measurements of resistivity with temperature. The semiconductivity in $LaCrO_3$ must be due to large oxygen deficiency in it. The material would then adsorb the oxygen species at higher temperatures ($O_2^- \rightarrow 2O^- \rightarrow O^{2-}$). The increase in conductivity with increasing temperature could be attributed to negative temperature coefficient of resistance and semiconducting nature of the $LaCrO_3$. It is observed from Fig. 6 that the electrical conductivity of the $LaCrO_3$ is nearly linear in the temperature range from 300–625 °K in air ambient.

5. Sensing Performance

5.1. Sensing Characteristics

The relative response to a target gas is defined as the ratio of the change in conductance of a sample upon exposure of the gas to the original conductance in air. The gas response can be written as:

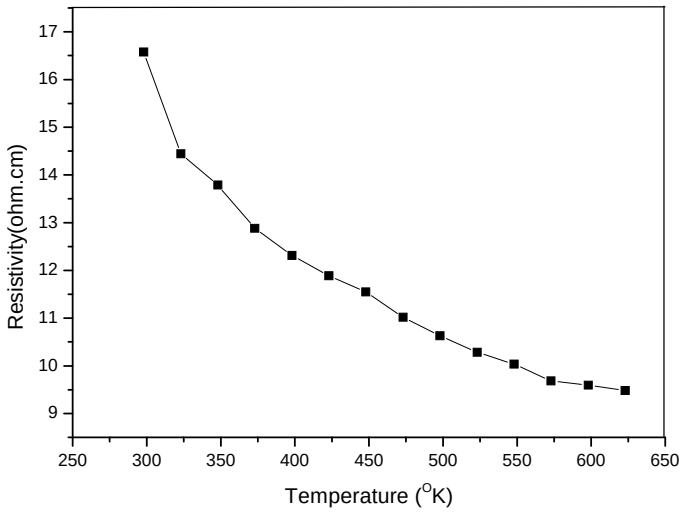

Fig. 6. Conductance-temperature profiles of $LaCrO_3$ sample in air.

$$\text{Gas Response} = \frac{G_g - G_a}{G_a} = \frac{G}{G_a},$$

where G_a is the conductance in air and G_g is the conductance in a sample gas. Specificity or selectivity can be defined as the ability of a sensor to respond to a certain gas in the presence of different gases. Response time (RST) was defined as the time required for a sensor to attain the 90 % of the maximum increase in conductance after the exposure of test gas on the sensor surface, while recovery time (RCT) as the time taken to get back 90 % of the maximum conductance in air.

5.2. Gas Response of $LaCrO_3$ at Various Temperatures

5.2.1. Gas Response and Operating Temperature

It is well known that the gas sensitivity is greatly influenced by operating temperature and the amount of additives. In order to determine the optimum operating temperature and additive amount, responses of $LaCrO_3$ sensors to acetone vapor were examined as a function of operating temperature. From Fig. 6, it can be seen that for 200 ppm acetone the maximum response values of $LaCrO_3$, at the optimal temperature of 200 °C, respectively. It indicates that $LaCrO_3$ exhibited the best sensing behavior for acetone vapour. The acetone vapor sensing mechanism is a complex process. It is based on the changes in resistance of materials which is controlled by the acetone vapor species and the amount of the chemisorbed oxygen on the surface [26-28]. The $LaCrO_3$ interacts with the oxygen, by transferring the electrons from the valence band to adsorbed oxygen atoms, forming ionic species such as O^{2-} or O^{-}. The electron transfer from the valence band to the chemisorbed oxygen results in an increase in hole concentration and a decrease in resistance of the $LaCrO_3$ based sensor. When the sensor is exposed to acetone vapor, the acetone vapor reacts with the chemisorbed oxygen, releasing electrons back to the valence band with an increase in resistance. The overall reaction of acetone vapor with chemisorbed oxygen may take place as below [29].

$$CH_3COCH_{3\,(gas)} + O^{-} \rightarrow CH_3C^{+}O + CH_3O^{-} + e^{-}$$
$$CH_3C^{+}O \rightarrow C^{+}H_3 + CO$$
$$CO + O^{-} \rightarrow CO_2 + e^{-}$$

At low temperature (lower than optimal temperature), the reaction products do not desorb from the sensor surface. The species cover the sensing sites on the sensor surface, which prevents the further reaction between acetone vapor and chemisorbed oxygen. Thus the resistance of the sensor increases little. At optimal temperature, the reaction products become desorbed, giving sensing sites on the sensor to react with new gas species. So acetone vapor reacts most effectively with chemisorbed oxygen at this temperature. The resistance of the sensor increases significantly. Therefore the highest response reaches. At temperature higher than the optimal temperature, the adsorbed gas begins to desorb. Less acetone vapor reacts with chemisorbed oxygen, which results in a small change in resistance of the sensor. The relationship between the resistance of $LaCrO_3$ based sensor and the acetone vapor concentration at the optimal temperature of 200 ^{0}C is shown in Fig. 7. The resistance increases significantly with an increase in acetone vapor concentration. [30-31]. It is clear from the Fig. 7 that the gas response increase with operating temperature reaches to the maximum (200 ppm) at 200 ^{0}C, and falls with further increasing the in operating temperature. The acetone may burn before reaching the surface of the film at higher temperatures (>200 ^{0}C). Hence, the gas response would have been decreased above 200 ^{0}C. A larger amount of oxygen-adsorption would have occurred on the surface of the film at 200 ^{0}C and have facilitated the sensor to oxidize the acetone gas immediately, giving faster and larger gas response.

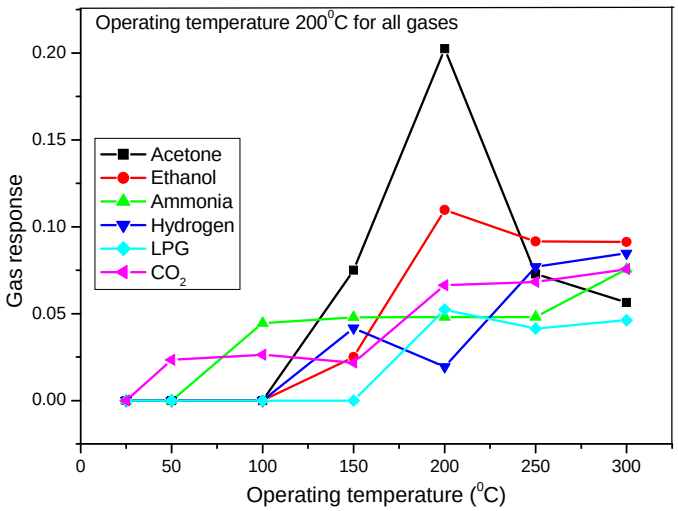

Fig. 7. Variation of gas response with operating temperature.

5.2.2. Acetone Gas Response and Gas Concentration

Fig. 8 represents the variation of acetone gas response with the gas concentration of $LaCrO_3$ film. For $LaCrO_3$ film, the response values were observed to increase continuously with increasing the gas concentration up to 200 ppm at 200 ^{0}C. The rate of increase in response was relatively larger up to 200 ppm, and then saturated after 200 ppm. Thus, the active region of the sensor would be between 30 and 200 ppm.

5.2.3. Selectivity for Acetone Against Various Gases

Fig. 9 depicts the selectivity of $LaCrO_3$ to 200 ppm of acetone gas against various gases at 200 ^{0}C. It is clear from Fig. 9 that, in contrast to pure $LaCrO_3$, the sample shows not only enhanced response towards acetone but also very high selectivity.

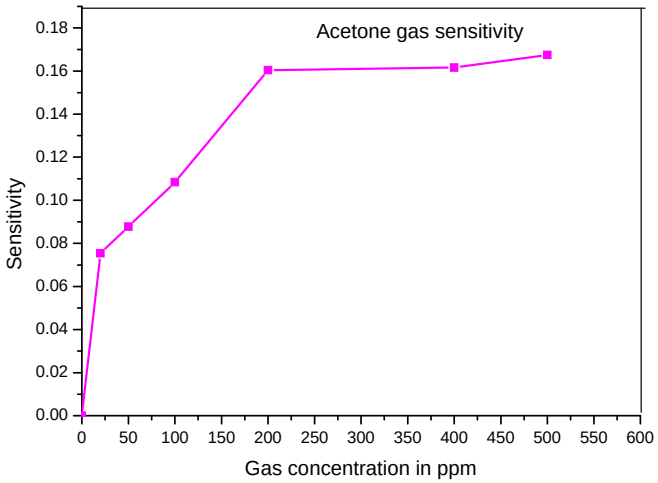

Fig. 8. Variation of gas response with gas concentration.

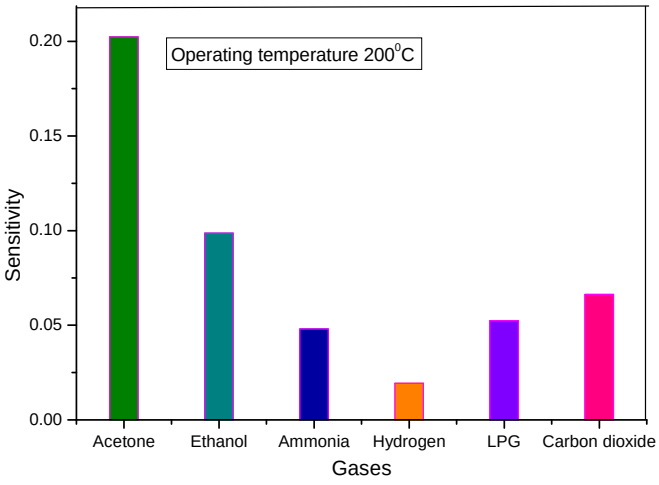

Fig. 9. Gas responses among various gases.

5.2.4. Response and Recovery of the Sensor

The response and recovery of the $LaCrO_3$ sensor are represented in Fig. 10. The response was quick (≈5 s) to 200 ppm of acetone. Recovery was also very fast (≈60 s). The fast response may be due to the fast oxidation of acetone into Hs_2O (gas). After evaporating water molecules, the film recovery was obtained.

7. Conclusion

The following statements can be made for the sensing performance of $LaCrO_3$ sensors:
(1) Pure $LaCrO_3$ thick film is the most sensitive element to acetone gas.
(2) The optimum operating temperature for acetone (200 ppm) gas sensing was 200 ^{0}C.
(3) $LaCrO_3$ has the potential of fabricating acetone sensor.
(4) The $LaCrO_3$ thick film sensor showed very rapid response and recovery to acetone gas.
(5) The sensor showed good selectivity to acetone gas against LPG, NH_3, C_2H_5OH, CO_2 and H_2 gases.
(6) The sensor was highly selective to a trace amount (200 ppm) of acetone gas from other toxic gases of higher concentrations.
(7) The sensor showed very rapid response (~5 s) and recovery (~60 s) to acetone gas.

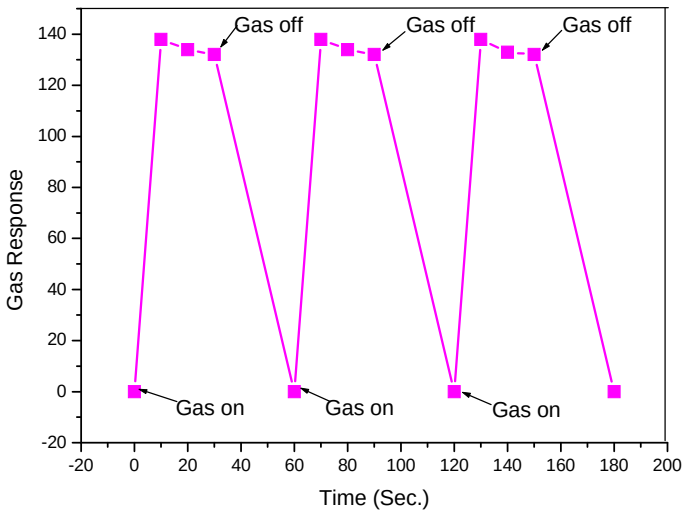

Fig. 10. Response and recovery of the $LaCrO_3$ sensor.

Acknowledgements

Authors are grateful to the Dr. D. R. Patil (Bulk and Nano material Laboratory, L. R. College Parola, Jalgoan) for useful discussion and support.

References

[1]. M. Yuasa, T. Masaki, T. Kida, K. Shimanoe, N. Yamazoe, Nano-sized PdO loaded SnO_2 nanoparticles by reverse micelle method for highly sensitive CO gas sensor, *Sensors and Actuators B,* 2009, 136, pp. 99–104.

[2]. M. Law, H. Kind, F. Kim, B. Messer, P. Yang, Preparation of tin oxide self assembly nanostructures by chemical, *Angew. Chem. Int. Ed*., 2002, 41, pp. 2405.

[3]. J. Chen, L. N. Xu, W. Y. Li, α-Fe_2O_3 nanotubes in gas sensor and lithium-ion battery applications, *Adv. Mater*., 2005, 17, pp. 582-586.

[4]. V. D. Kapse, S. A. Ghosh, G. N. Chaudhari, F. C. Raghuwanshi, H_2S sensing properties of La-doped nanocrystalline In_2O_3, *Vacuum*, 2008, 83, pp. 346-352.

[5]. R. C. Biswa, Pure and Pt-loaded gamma iron oxide as sensor for detection of sub ppm level of acetone, *Sensors and Actuators B,* 2011, 157, pp. 183– 188.

[6]. T. Cheng, Z. Y. Fang, Q. X. Hu, K. D. Han, X. Z. Yang, Y. J. Zhang, Low-temperature CO oxidation over CuO/Fe_2O_3 catalysts, *Catal. Commun,* 2007, 8, pp. 1167-1171.

[7]. P. A. Murade, V. S. Sangawar, G. N. Chaudhari, V. D. Kapse, A. U. Bajpeyee, Acetone gas-sensing performance of Sr-doped nanostructured $LaFeO_3$ semiconductor prepared by citrate sol-gel route, *Current Applied Physics*, 2011, 11, pp. 451-456.

[8]. S. B. Khan, M. Faisal, M. M. Rahman, A. Jamal Low-temperature growth of ZnO nanoparticles: Photocatalyst and acetone sensor, *Talanta*, 2011, 85, pp. 943– 949.

[9]. N. N. Toan, S. Saukko, V. Lantto, Gas sensing with semiconducting perovskite oxide $LaFeO_3$, *Phys. B. Condens. Matter*, 2003, 327, pp. 279-282.

[10]. L. Malavasi, C. Tealdi, G. Flor, G. Chiodelli, V. Cervetto, A. Montenero, M. Borella, $NdCoO_3$ perovskite as possible candidate for CO-sensors: thin films synthesis and sensing properties, *Sens. Actuators B Chem*., 2005, 105, pp. 407-411.

[11]. G. Martinelli, M. C. Carotta, M. Ferroni, Y. Sadaoka, E. Traversa, Screen-printed perovskite-type thick films as gas sensors for environmental monitoring, *Sens. Actuators B Chem*., 1999, 55, pp. 99- 110.

[12]. Y. D. Wang, J. B. Chen, X. H. Wu, Preparation and gas-sensing properties of perovskite-type $SrFeO_3$ oxide, *Mater. Lett*., 2001, 49, pp. 361-364.

[13].D. R. Patil, L. A. Patil, Cr_2O_3-modified ZnO thick film resistors as LPG sensors, *Talanta*, 2009, 77, pp. 1409–1414.
[14].X. Liu, H. Ji, Y. Gu, M. Xu, Preparation and acetone sensitive characteristics of nano-$LaFeO_3$ semiconductor thin films by polymerization complex method, *Materials Science and Engineering B*, 2006, 133, pp. 98–101.
[15].Y. D. Wang, X. H. Wu, Su Q, Y. F. Lee, Z. L. Zhou, Ammonia sensing characteristics of Pt and SiO_2 doped SnO_2 materials, *Solid-State Electron*., 2001, 45, pp. 347-350.
[16].S. M. Khetre., H. V. Jadhav, P. N. Jagadale, S. R. Kulal and S. R. Bamane., Studies on electrical and dielectric properties of $LaFeO_3$, *Advances in Applied Science Research*, 2011, 2, 4, pp. 503-511.
[17].S. V. Patil, P. R. Deshmukh, C. D. Lokhande, Fabrication and liquefied petroleum gas (LPG) sensing performance of p-polyaniline/n-PbS heterojunction at room temperature, *Sensors and Actuators B*, 2011, 156, pp. 450–455.
[18].J. K Srivastava, P. Pandey, V. N. Mishra, R. Dwivedi, Sensing mechanism of Pd-doped SnO_2 sensor for LPG detection, *Solid State Sciences*, 2009, 11, pp. 1602–1605.
[19].S. V. Bangale, S. M. Khetre, D. R. Patil, S. R. Bamane, Simple Synthesis of $ZnCo_2O_4$ Nanoparticles as Gas-sensing Materials, *Sensors & Transducers*, 2011, Vol.134, Issue 11, pp. 95-106.
[20].G. V. S. Rao, C. N. R. Rao, Ferraro J. R., *Appl. Spectroscopy*., 1970, 24, pp. 436.
[21].H. M. Zhange, Y. Teraoka., N. Yamazoe., *Chem. Lett.,* 1987, p. 665.
[22].K. Nakamoto, Infrared and Raman Spectra of Inorganic and Coordination Compounds, 4th ed., *Wiley*, New York, 1986, pp. 252.
[23].Y. Sadaoka, K. Watanabe, Y. Sakai, M. Sakamoto, Preparation of perovskite-type oxides by thermal decomposition of heteronuclear complexes, $\{Ln[Fe(CN)_6]\cdot nH_2O\}_x$, (Ln = LaHo), *J. Alloys Compd*., 1995, 224, pp. 194-198.
[24].D. W. Johnson, P. K. Gallagar, F. Schrey, W. W. Rhodes., The nature and effects of platinum in perovskite catalysts, *Ceram. Bull*., 1976, 55, pp. 520.
[25].Y. Shimizu., M. Egashira, Mesoporous semiconducting oxides for gas sensor application, *Journal of the European Ceramic Society*, 2004, 24, 6, pp. 1389-1398.
[26].P. P. Sahay, Zinc oxide thin film gas sensor for detection of acetone, *J. Mater. Sci*., 2005, 40, pp. 4383–4385.
[27].D. E. Dyshel, T. F. Lobunets, A. A. Rogozinskaya, Porous structure of powders prepared with heat treatment of gels from tin(IV) and antimony(III) hydroxides, *Powder Metall. Met. Ceram.,* 2001, 40, pp. 1–7.
[28].K. Arshak, I. Gaidan, Gas sensing properties of $ZnFe_2O_4$/ZnO screen-printed thick films, *Sens. Actuators B*., 2005, 111–112, pp. 58-62.
[29].R. S Khadayate, J. V. Sali, P. P. Patil, Acetone vapor sensing properties of screen Printed WO_3 thick films, *Talanta*, 2007, 72, pp. 1077–1081.
[30].Y. C. Chen., Y. H. Chang, G. J Chen, Y. L. Chai, D. T. Ray, The sensing properties of heterojunction $SnO_2/La_{0.8}Sr_{0.2}Co_{0.5}Ni_{0.5}O_3$ thin-film CO sensor, *Sens. Actuators B,* 2003, 96, pp. 82–87.
[31].J. Watson, K. Ihokura, G. S. V Coles., The tin oxide gas sensor, *Meas. Sci. Technol.,* 1993, 4, pp. 711– 719.
